JOURNAL OF SOLID STATE CHEMISTRY 39, 173–180 (1981)

Formation of High Oxide Ion Conductive Phases in the Sintered Oxides of the System Bi_2O_3–Ln_2O_3 (Ln = La–Yb)

H. IWAHARA, T. ESAKA, AND T. SATO

Department of Environmental Chemistry and Technology, Faculty of Engineering, Tottori University, Minami 4-101, Koyama-cho, Tottori 680, Japan

AND T. TAKAHASHI

Department of Applied Chemistry, Faculty of Engineering, Nagoya University, Nagoya 464, Japan

Received November 29, 1980; in revised form March 23, 1981

The electrical conduction in various phases of the system Bi_2O_3–Ln_2O_3 (Ln = La, Nd, Sm, Dy, Er, or Yb) was investigated by measuring ac conductivity and the emf of the oxygen gas concentration cell. High-oxide-ion conduction was observed in the rhombohedral and face-centered cubic (fcc) phase in these systems. The fcc phase could be stabilized over a wide range of temperature by adding a certain amount of Ln_2O_3. In these cases, the larger the atomic number of Ln, the lower the content of Ln_2O_3 required to form the fcc solid solution, except in the case of Yb_2O_3. The oxide ion conductivity of this phase decreased with increasing content of Ln_2O_3. Maximum conductivity was obtained at the lower limit of the fcc solid solution formation range in each system, which was more than one order of magnitude higher than those of conventional stabilized zirconias. Lattice parameters of the fcc phase were calculated from the X-ray diffraction patterns. The relationship between the oxide ion conductivity and the lattice parameter was also discussed.

1. Introduction

The high-temperature phase (δ phase) of bismuth sesquioxide is known to show the defect fluorite-type (fcc) crystal structure and to be a highly conductive oxide ion conductor (*1–3*). This phase is, however, unstable below 730°C and transforms to the monoclinic phase (α phase), whose conduction is low and electronic. Previously, we reported that a highly conductive phase could be retained far below 730°C by adding certain di-, tri-, penta- or hexavalent metal oxides (*4, 5*). In these binary oxide systems, the oxide ion conductive phase is of fcc type, corresponding to the δ form of pure Bi_2O_3, or of rhombohedral type analogous to that of the system Bi_2O_3–SrO, reported by Sillen *et al.* (*6*). The oxide ion conductive phase in the Bi_2O_3–Y_2O_3 system belongs to the former (*7*), whereas that in the Bi_2O_3–La_2O_3 system belongs to the latter type (*8*). The system Bi_2O_3–Gd_2O_3 gives both fcc and rhombohedral phases which are good oxide ion conductors (*9*). Recently, Verkerk *et al.* reported the presence of a high oxide ion conductive fcc phase in the system Bi_2O_3–Er_2O_3 (*10*).

0022-4596/81/110173-08$02.00/0

Considering the cationic radius of added oxides, we can expect that the oxide ion conductive phase in the system Bi_2O_3–M_2O_3 is rhombohedral in the case of a relatively large ionic radius of M^{3+} and is fcc in the case of a comparatively small radius of M^{3+}. The compound M_2O_3 having a cationic radius of medium size may be anticipated to oxide ion conductors both in fcc and rhombohedral phases, depending on its composition.

The series of lanthanide elements, *Ln*, has chemical properties similar to each other, but their cationic radii increase from 1.18 Å for La^{3+} to 0.97 Å for Lu^{3+} with increasing atomic number (*11*). The crystal phases present in the system Bi_2O_3–Ln_2O_3 are expected to change with the cationic radii, and, therefore, the oxide ion conductive phase will vary as the atomic number of *Ln* changes. Although the phase diagrams of Bi_2O_3–Ln_2O_3 are partly published, the composition ranges studied are rather narrow and are often limited to the Bi_2O_3-rich region (>90 mole% Bi_2O_3) in most cases (*12, 13*). In the present study, we investigated both electrical conduction and crystal phases in the series Bi_2O_3–Ln_2O_3 (*Ln* = La, Nd, Sm, Dy, Er, or Yb) in relation to ionic radii of the lanthanide ions and their compositions.

2. Experimental

2.1. Preparation of Samples

The starting materials used were bismuth sesquioxide and rare-earth oxides. The former was obtained by thermal decomposition of $Bi(NO_3)_3 \cdot 5H_2O$ (JIS special grade) at 700°C. The purity of the latter was higher than 99.9%.

The powders were mixed and calcined at 800–1100°C for 10 hr in air, then they were finely ground and pressed hydrostatically into the shape of a rod (4–6 mm ø × 8–10 mm) or disk (10 mm ø × 2–3 mm) under 2 tons/cm² and sintered again in air for 10 hr. The temperature for sintering is shown in Table I. In order to prepare dense specimens, the sintering temperature was raised as the content of rare-earth oxide increased.

Each crystal phase of sample was identified by X-ray diffraction at room temperature using Cu$K\alpha$-radiation with a nickel filter. The lattice parameters were calculated from the diffraction angles of each peak obtained by slow scanning speed ($\frac{1}{4}$° min^{-1}) using NaCl as an internal standard.

2.2. Measurement of Ionic Conduction

Ionic conduction in the sintered specimens was examined by measuring the electrical conductivity and the emf of oxygen gas concentration cells using specimen disks as electrolytes. Electrical conductivity was measured in air using the two-probe ac method. The frequency used was 1–10 kHz. Porous silver or platinum powder was adopted as the electrode material. The paste of each metal was smeared on the faces of the specimen disk and fired at 800°C. The platinum was mainly used for the Bi_2O_3-rich specimens (~10 mole% Ln_2O_3), which were somewhat reactive with silver paste at higher temperatures. In order to determine the ionic transport number, the emf of the following oxygen concentration cell was measured,

TABLE I

SINTERING TEMPERATURE OF $(Bi_2O_3)_{1-x}(Ln_2O_3)_x$

Ln_2O_3 (x)	Temperature (°C)
0.05–0.10	850
0.20	950
0.30	1000
0.40	1100
0.50	1150

$O_2(P_{O_2},a)$,Ag/specimen
disk/Ag,$O_2(P_{O_2},c)$. (1)

If the conduction in the specimen is predominantly ionic, the emf of the cell E_0 is given by

$$E_0 = (RT/4F)\ln(P_{O_2},c/P_{O_2},a) \quad (2)$$

where R, T, and F have their usual meanings and P_{O_2}, a and P_{O_2}, c are oxygen partial pressures at anode and cathode, respectively. If the specimen has some electronic conduction as well as ionic conduction, the emf will lower from E_0 to some extent because of the discharge of the cell due to electronic conduction. Here, pure oxygen at 1 atm was used as cathode gas and air as anode gas. The design of the cell as well as these general procedures were the same as those previously reported (*5*, *7–9*).

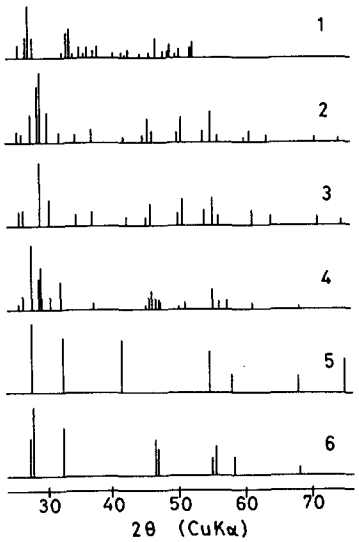

FIG. 1. X-Ray diffraction patterns of $(Bi_2O_3)_{1-x}(Sm_2O_3)_x$ annealed from the sintering temperature to room temperature. (1) $x = 0.0$; (2) $x = 0.20$; (3) $x = 0.30$; (4) $x = 0.35$; (5) $x = 0.40$; (6) $x = 0.50$.

3. Results

3.1. Specimen Preparation

The specimens thus prepared were well sintered and had no open pores to allow the penetration of gas. The color of specimens was orange for 10–20 mole% Ln_2O_3 and turned yellowish with increasing Ln_2O_3 content, except for the specimens of the system Bi_2O_3–Nd_2O_3, the color of which was greenish over the whole composition range of Nd_2O_3.

Figure 1 represents the X-ray diffraction patterns of the specimens having the representative compositions in the system Bi_2O_3–Sm_2O_3. These specimens were annealed from the sintering temperature to room temperature in order to avoid freezing of high-temperature crystal forms. Besides the monoclinic Bi_2O_3, three types of single phase are observed:

(1) the rhombohedral single phase for 30 mole% Sm_2O_3, which corresponds to the rhombohedral crystal system reported in the system Bi_2O_3–SrO by Sillen *et al.* (*6*).

(2) the fcc single phase for 40 mole% Sm_2O_3, which is analogous to pure δ-Bi_2O_3.

(3) LaOF-type rhombohedral phase (*15*) for 50 mole% Sm_2O_3. The specimens of the other compositions show the mixed phases of the corresponding phases. However, when the specimens were quenched from the sintering temperature, all the specimens containing less than 40 mole% Sm_2O_3 showed the fcc form, suggesting that the fcc phase is stable at high temperatures in a wide range of composition (~40 mole% Sm_2O_3). The fcc phase stable over a wide range of temperature is present only around the composition at 40 mole% Sm_2O_3. These results are similar to those of the system Bi_2O_3–Gd_2O_3 reported previously (*9*). In the present experiment, the LaOF-type rhombohedral phase was newly observed as a stable crystal phase in the Bi_2O_3-based system. Although this was considered to be a somewhat distorted fcc phase, the detailed investigation was not carried out here. The relation between the crystal phase and the composition in other systems are summarized in Table II.

TABLE II

THE CRYSTAL PHASE OBSERVED IN THE ANNEALED AND THE QUENCHED SPECIMENS OF $(Bi_2O_3)_{1-x}(Ln_2O_3)_x$

Ln_2O_3		Crystal phase observed[a]	
Ln	*x*	Annealed specimen	Quenched specimen
La	0.15–0.28	rhomb	rhomb
	0.30–0.40	rhomb + LaOF	
	0.50	LaOF	
Nd	0.10–0.30	rhomb	rhomb + fcc
	0.40	rhomb + LaOF	
	0.50	LaOF	
Sm	0.10–0.20	rhomb + ?	fcc
	0.30	rhomb	fcc
	0.35	rhomb + fcc	fcc
	0.40	fcc	
	0.50	LaOF	
Dy	0.20	rhomb + ?	fcc
	0.30–0.40	fcc	
Er	0.20	fcc + ?	fcc
	0.25–0.30	fcc	
Yb	0.10	tetra	fcc + ?
	0.20	tetra + ?	fcc
	0.30	fcc	
	0.40	fcc + ?	

[a] fcc = face-centered cubic phase corresponding to δ phase of Bi_2O_3; rhomb = rhombohedral phase; tetra = tetragonal phase; LaOF = LaOF-type rhombohedral phase; ? = unidentified.

Figure 2 shows the relations between the lattice parameters of fcc phases and the compositions for various rare-earth oxide dopants. As the fcc phases were not stable at room temperature in the content ranges of Ln_2O_3 lower than those indicated by the dashed lines, we calculated the lattice parameters in those cases by using the quenched samples. They obey Vegard's rule in all cases.

3.2. Conductivity

Figure 3 shows the representative Arrhenius plots of conductivity measured in air

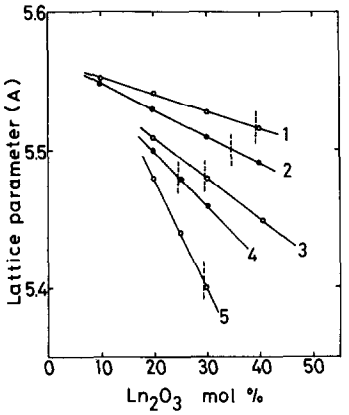

FIG. 2. Lattice parameters of fcc phases in $(Bi_2O_3)_{1-x}(Ln_2O_3)_x$. (1) *Ln* = Sm; (2) *Ln* = Gd; (3) *Ln* = Dy; (4) *Ln* = Er; (5) *Ln* = Yb.

for the sintered specimens of the system Bi_2O_3–Sm_2O_3. As indicated with a broken line, pure Bi_2O_3 shows an abrupt conductivity jump in which the phase transition from monoclinic to fcc phase takes place. The analogous but more gradual conductivity increase is observed in the sintered specimens containing less than 35 mole% Sm_2O_3. DTA of these specimens showed the endothermic change at those temperatures. From considerations of X-ray diffrac-

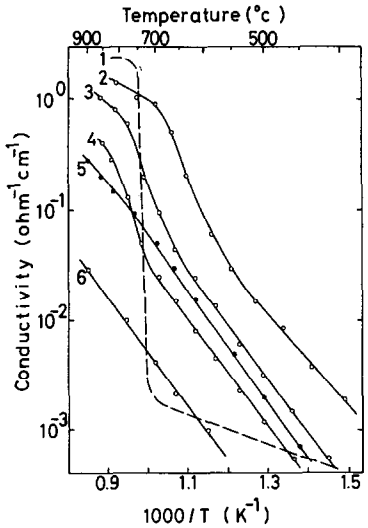

FIG. 3. Arrhenius plots of conductivity for sintered oxides of $(Bi_2O_3)_{1-x}(Sm_2O_3)_x$. (1) $x = 0.0$; (2) $x = 0.10$; (3) $x = 0.20$; (4) $x = 0.30$; (5) $x = 0.40$; (6) $x = 0.50$.

tion patterns and the results of DTA, the abrupt conductivity increase was ascribed to the phase transition from rhombohedral (low-temperature form) to fcc phase (high-temperature form). The Sm_2O_3-rich specimens (more than 40 mole%) showed no conductivity jump and the Arrhenius plots of conductivity showed an almost linear relation over the whole range of temperature measured. This means that the fcc single phase is stable from room temperature to high temperature (~900°C).

Other present systems of Bi_2O_3–Ln_2O_3 (Ln = La, Nd, Dy, Er, and Yb) showed conductivity properties analogous to those of the Bi_2O_3–Sm_2O_3 system. However, the high-temperature phase was not always fcc (see Table II). The rhombohedral samples having low contents of La_2O_3 did not show obvious difference in the X-ray diffraction patterns between annealed and quenched oxides, but conductivity jumps appeared in the Arrhenius plots. In this case, a different phase was not observed even by high-temperature X-ray diffraction up to 800°C. This suggests that the jump in conductivity is ascribed to the order–disorder transition in the rhombohedral phase, as reported in Ref. (*14*) for the case of Bi_2O_3–SrO. Minimum contents of doped oxides to show no conductivity jump corresponded to those of formation of fcc phase stable at lower temperatures except the systems Bi_2O_3–La_2O_3 and Bi_2O_3–Nd_2O_3, where the fcc phase was not observed even if the linear conductivity vs $1/T$ relations were present. These relationships between formation of the fcc phase and linearity of the Arrhenius plots observed in the systems Bi_2O_3–Ln_2O_3 (Ln = Sm, Dy, Er, and Yb) were the same as those in the case of Y_2O_3- or Gd_2O_3-doped Bi_2O_3 (*7, 9*).

Verkerk *et al.* recently reported the conduction properties in the system Bi_2O_3–Er_2O_3 (*10*), where the lower limit of Er_2O_3 content to form the fcc single phase and the content without showing a conductivity jump were 17.5 and 20 mole%, respectively. These results are partly different from our result, which show both lower limits are 25 mole% Er_2O_3.

TABLE III

RATIOS OF THE MEASURED EMF TO THE THEORETICAL VALUE E_0 OF THE CELL O_2(0.21 ATM), $Ag/(Bi_2O_3)_{1-x}(Ln_2O_3)_x/Ag,O_2$(1.0 ATM)

Ln_2O_3		E/E_0			
Ln	*x*	500°C	600°C	700°C	800°C
La	0.20	0.96	0.95	0.94	—
Nd	0.20	0.98	0.99	0.96	0.97
Sm	0.20	1.00	0.96	0.97	0.97
	0.40	0.94	0.92	0.93	0.93
Dy	0.30	0.96	0.97	0.98	0.98
Er	0.25	1.02	0.99	1.00	0.99
Yb	0.10	0.86	0.78	0.83	—
	0.30	—	0.95	0.96	0.96

The ratios of the measured emf to the theoretical value in the oxygen gas concentration cell for representative specimens were shown in Table III. Besides the case of 10 mole% Yb_2O_3-doped tetragonal oxide, the specimens having a certain amount of Ln_2O_3 show the values above 0.90 even in the temperature range below 700°C, where the essential charge carrier in pure Bi_2O_3 is an electron hole, denoting that ionic conduction is predominant over a wide range of temperature.

The steady current could be drawn out from these oxygen concentration cells, as shown in Fig. 4. The dc resistance calculated from the I–V relation of the cell was almost comparable to the value measured by an ac bridge in each case. These results indicate that the conductive ions should be oxide ions. Therefore, the conductivities measured in this experiment are to show oxide ion conductivities. Oxide ion conductivities of these systems are generally higher than those of stabilized zirconias. Especially rhombohedral $(Bi_2O_3)_{0.85}(La_2O_3)_{0.15}$, rhombohedral $(Bi_2O_3)_{0.90}(Nd_2O_3)_{0.10}$, and cubic $(Bi_2O_3)_{0.75}$

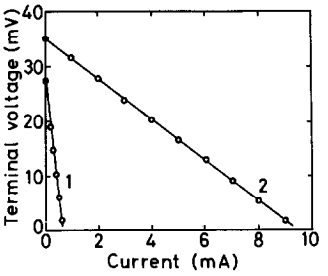

FIG. 4. Terminal voltage versus discharge current relations of the cell O_2(0.21 atm), Ag/$(Bi_2O_3)_{0.60}(Sm_2O_3)_{0.40}$/Ag,$O_2$(1.0 atm); (1) 600°C; (2) 800°C.

$(Er_2O_3)_{0.25}$ oxides are the highest oxide ion conductivity conductors. In Fig. 5 the conductivities of these specimens are shown in Arrhenius plots. They are more than 10 times higher than that of conventional stabilized zirconia like $(ZrO_2)_{0.90}(Y_2O_3)_{0.10}$.

4. Discussion

Figure 6a shows the isothermal conductivity vs the content of Ln_2O_3 relation at 800°C. In this high-temperature range the conductivity decreases monotonously with increasing content of Ln_2O_3 and the conductivity in the Ln_2O_3-rich samples is almost independent of the kind of Ln. In the low-temperature range, these systems can be divided into two groups; one has maxima in conductivity and another has monotonous variations as shown in Fig. 6b. The systems with the fcc phase belong to the former, whereas the systems without the fcc phase belong to the latter. The composition with maximum conductivity corresponds to the lower limit of the fcc solid-solution formation range stable at lower temperatures in each system. Except for the case of Yb_2O_3, this composition is relative to the atomic number of Ln; the larger the atomic number of Ln (that is, the smaller the ionic radius of Ln^{3+}), the lower the content of Ln_2O_3 required to stabilize the fcc phase at lower temperatures. In the rhombohedral phase of the systems Bi_2O_3–Ln_2O_3 (Ln = La, Nd, Sm, and Gd), the highest conductivity was also found at the lower limit of Ln_2O_3 content.

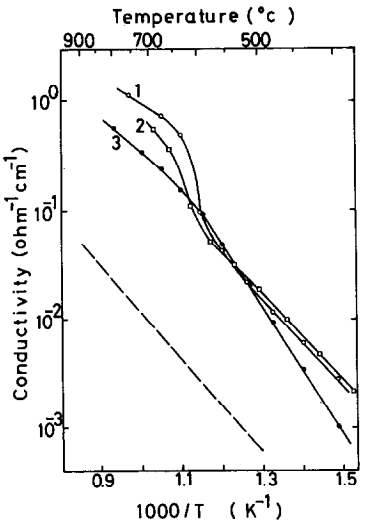

FIG. 5. Arrhenius plots of conductivity of sintered oxides of the system Bi_2O_3–Ln_2O_3: (1) $(Bi_2O_3)_{0.90}(Nd_2O_3)_{0.10}$; (2) $(Bi_2O_3)_{0.85}(La_2O_3)_{0.15}$; (3) $(Bi_2O_3)_{0.75}(Er_2O_3)_{0.25}$. The broken line shows the conductivity of the stabilized zirconia $(ZrO_2)_{0.9}(Y_2O_3)_{0.1}$ for reference.

The lower limits for stable fcc phase are shown as dashed lines in Fig. 2 which represents the lattice parameter of fcc phase vs the content of Ln_2O_3 relations. The lattice parameters of the fcc phase at the lower limit increase with increasing ionic radius of Ln^{3+}. The peculiar behavior of Yb_2O_3-doped specimens in Fig. 2 as well as in Fig. 6b could not be made clear in this investigation. Probably, considering the abnormal properties of the Yb atomic radius compared with the other rare-earth elements, the special electron configuration of Yb itself might contribute to the peculiar electrical and structural properties.

The isothermal conductivities for only the fcc phase in Fig. 6b are shown again in Fig. 7. They lie almost on a straight line, irrespective of the kind of Ln. Accordingly, the conductivities are to depend almost

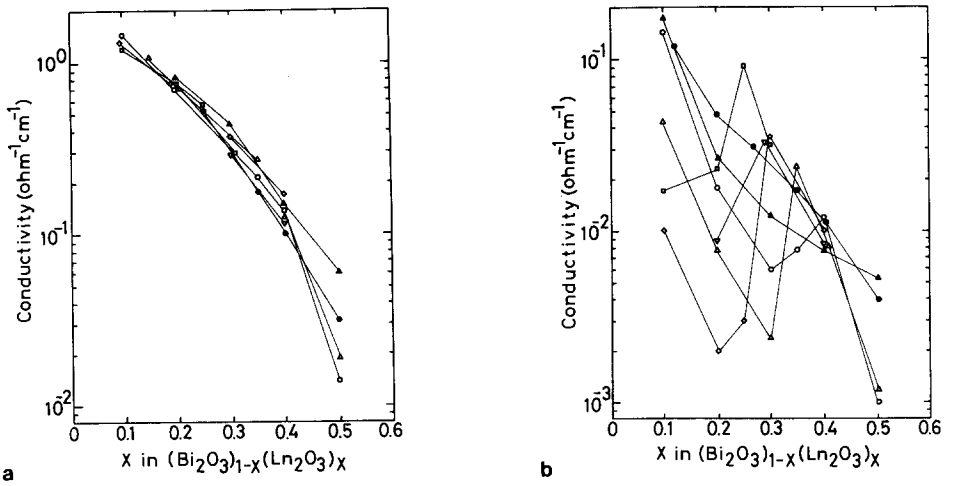

FIG. 6. Isothermal conductivity of the system $(Bi_2O_3)_{1-x}(Ln_2O_3)_x$ at 800°C (a) and 600°C (b). ●, Ln = La; ▲, Ln = Nd; ○, Ln = Sm; △, Ln = Gd; ▽, Ln = Dy; □, Ln = Er; ◇, Ln = Yb.

exclusively on the content of Ln_2O_3, although the lattice parameters at the same composition differ obviously as shown in Fig. 2. In other words, the oxide ion conduction in the fcc phase seems to be provided not so much by the jump length of the oxide ion corresponding to the lattice parameter, but almost only by the concentration of the doped Ln_2O_3. Considering this together with the result of Fig. 2, if a M^{3+} smaller than that examined here were used, the oxide content required to stabilize the fcc phase would be much less and the resultant oxide ion conductivity would be much higher.

Figure 8 shows the regions of fcc and rhombohedral phases stable at room temperature in relation to the ionic radius of Ln^{3+} and its content. The ionic radii for eight-fold coordination by Shannon *et al.* (*11*) were adopted here. The broken lines

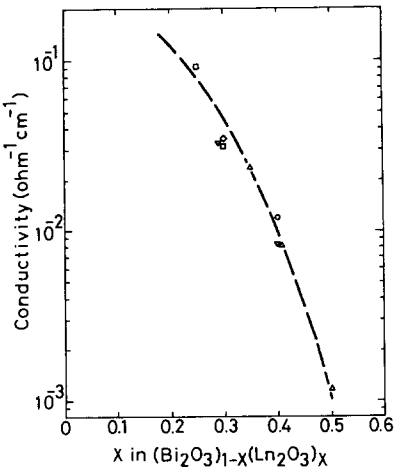

FIG. 7. Isothermal conductivity in the fcc phase of the system $(Bi_2O_3)_{1-x}(Ln_2O_3)_x$ at 600°C: ○, Ln = Sm; △, Ln = Gd; ▽, Ln = Dy; □, Ln = Er; ◇, Ln = Yb.

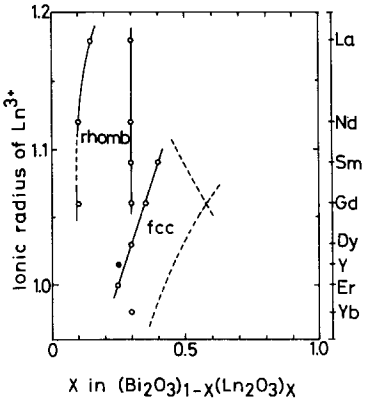

FIG. 8. Formation range of the rhombohedral and fcc phases in the ionic radius of Ln^{3+} versus composition diagram; rhomb = rhombohedral phase and fcc = face-centered cubic phase corresponding to δ-Bi_2O_3.

show some uncertainty due to the rough examination in relatively low and high contents of Ln_2O_3. The rhombohedral phase is formed in the low-content region of the systems doped with La_2O_3, Nd_2O_3, Sm_2O_3, and Gd_2O_3, the cationic radii of which are comparatively large. The fcc phase is stabilized by doping the oxides with relatively smaller cationic radii than Bi^{3+}. The lower limit of Ln_2O_3 content to form the fcc phase varied directly with the ionic radius of Ln^{3+} except in the case of Yb, showing that the smaller the ionic radius of Ln^{3+}, the lower the content required to stabilize the fcc phase. A solid circle indicates the datum of the system Bi_2O_3–Y_2O_3, reported in Ref. (*7*), for reference. The slight deviation from a straight line was considered to be due to the difference of the electronic configuration of Y (*5d*) and *Ln* (*5f*).

5. Conclusion

The rhombohedral and fcc single phases in the systems Bi_2O_3–Ln_2O_3 (*Ln* = La–Yb) were found to show high oxide ion conductivity. The rhombohedral phase appeared in the case of Ln^{3+} of a relatively large ionic radius. The fcc phase could be stabilized by adding Ln^{3+} ions with a cationic radius smaller than that of Bi^{3+}. Besides the case of Yb, the smaller the ionic radius of Ln^{3+}, the lower the Ln_2O_3 content required to stabilize the fcc phase. The oxide ion conductivity decreased with increasing content of dopant. Maximum conductivity was observed at the lower limit of the fcc solid-solution formation range in each case, which was more than one order of magnitude higher than those of well-known stabilized zirconias. The conductivity in the fcc phase was governed by the content of Ln_2O_3 and almost independent of the kind of *Ln*. Consequently, the lower the content of Ln_2O_3, the higher the oxide ion conductivity. The rhombohedral specimens containing 15 mole% La_2O_3 or 10 mole% Nd_2O_3 also showed somewhat higher values than did those of the above fcc oxides at lower temperatures. Considering these results, we might be able to obtain a higher oxide ion conductivity than those examined here if these single phases could be stabilized by adding a smaller amount of other oxides.

References

1. R. S. Sethi and H. C. Gaur, *Indian J. Chem.* **3**, 177 (1955).
2. M. G. Hapase and V. B. Tare, *Indian J. Pure Appl. Phys.* **5**, 401 (1967).
3. H. A. Harwig and A. G. Gerards, *J. Solid State Chem.* **26**, 265 (1978).
4. T. Takahashi and H. Iwahara, *Mater. Res. Bull.* **13**, 1447 (1978).
5. T. Takahashi, H. Iwahara, and T. Esaka, *J. Electrochem. Soc.* **124**, 1563 (1977).
6. L. G. Sillen and B. Aurivillius, *Z. Kristallogr.* **101**, 483 (1939).
7. T. Takahashi, H. Iwahara, and T. Arao, *J. Appl. Electrochem.* **5**, 187 (1975).
8. T. Takahashi, H. Iwahara, and Y. Nagai, *J. Appl. Electrochem.* **2**, 97 (1972).
9. T. Takahashi, T. Esaka, and H. Iwahara, *J. Appl. Electrochem.* **5**, 197 (1975).
10. M. J. Verkerk, K. Keizer, and A. J. Burggraaf, *J. Appl. Electrochem.* **10**, 81 (1980).
11. R. D. Shannon and C. T. Prewitt, *Acta Crystallogr. Sect. B* **25**, 925 (1969).
12. E. M. Levin and R. S. Roth, *J. Res. Nat. Bur. Standards A* **68**, 200 (1964).
13. R. K. Datta and J. P. Meehan, *Z. Anorg. Allg. Chem.* **383**, 328 (1971).
14. T. Takahashi, T. Esaka, and H. Iwahara, *J. Solid State Chem.* **16**, 317 (1976).
15. W. H. Zachariasen, *Acta Crystallogr.* **4**, 231 (1951).